Orbit Modeling of Asteroid 2017 BM31

Yale Summer Program in Astrophysics

Emma Arsekin
Harmony School of Advancement

Parker Jochum
Trinity Preparatory School

Kiki Huang
Shanghai American School

Shawn Zhang
Amador Valley High School

5 August 2017

Abstract

This four-week research project focused on mapping the orbit and determining the physical characteristics of the small near-Earth asteroid, 2017 BM31, a recently discovered asteroid with few astrometric observations. Using remote observations in addition to in-person imaging from the Leitner Family Observatory and Planetarium, we produced series of measurable images which we analyzed using the image processing softwares MaxIm DL and SAOImage DS9. With this data, our team tracked BM31's orbital elements over the course of three weeks and then performed further photometric analysis to provide insight into its size and composition. Our results show that the asteroid's perihelion point is 0.98 AU away, its eccentricity is 0.15, and its inclination is 21.6°. Furthermore, we created an optimized orbit model in Python that integrated BM31's motion forwards in time, revealing that its path takes it just outside the Earth's orbit, but at a velocity that would produce a larger blast than any nuclear weapon should it collide with the Earth.

1 Introduction

While they may not seem intimidating, even relatively small asteroids can cause massive damage upon impact with the Earth; the twenty-meter Chelyabinsk meteor impact in February 2013, for example, caused glass to shatter within a 120-kilometer radius of the meteor's shockwave and led to hundreds of reported injuries (Popova et al. 2013). This makes it imperative to understand and predict the movements of near-Earth asteroids such as 2017 BM31, an extremely small, fast-moving asteroid with low apparent magnitude. These characteristics make it difficult to track and even locate in the night sky, leading our team to conduct multiple observations from telescopes in Spain, Australia, and California to supplement our data from the Leitner Observatory in New Haven. These telescopes produced images that we could then measure, allowing us to incorporate our astrometric data into a Python simulation using the method

of Gauss. By integrating BM31's position in space over time, we created an accurate orbit model projecting well into the future. This allowed us to easily visualize the asteroid's path and determine the probability of a collision within the next hundred thousand years.

2 Methods

2.1 Data Collection and Analysis

Over the course of three weeks, our team conducted observations of 2017 BM31 from the Leitner Family Observatory and Planetarium's 16-inch reflecting telescope in New Haven, Connecticut. To supplement these images, we also conducted remote observations from the Siding Spring Observatory in Australia, the AstroCamp Observatory in Spain, and the Auberry telescope in California via *itelescope.net*. After imaging the sky with these telescopes, the photos were analyzed with MaxIm

DL (Version 3.04; George et al. 2001) and SAOImage DS9 (Version 7.4; Joye et al. 2015), programs that are able to analyze and manipulate astrometrical images.

Once our data had been collected, our team blinked through sets of nightly images in MaxIm DL and was able to—with considerable difficulty for our faint asteroid—identify 2017 BM31 and observe its path as it streaked across the sky. We prepared our images for analysis by solve-fielding them using *astrometry.net* (Lang et al. 2010), which matches the images we took against a catalog of star patterns across the sky. The program then identifies reference stars it can use to map the right ascension (α) and declination (δ) equivalents of every pixel in the image, generating a World Coordinate System (WCS). We also wrote a Python program implementing the least squares plate reduction method to use reference stars to generate a right ascension-declination map for the image; however, because *astrometry.net*'s algorithms are more extensive and accurate, we ultimately used them to obtain the right ascension and declination of our asteroid for all of our observations.

Much of our data collection and analysis was complicated by the dimness of our asteroid. Its low magnitude made it nearly impossible to spot in some of our shorter exposure images, and it moved too quickly to appear as anything but a dim streak that could not be centroided in longer exposures. We circumvented this problem by ceasing to use MaxIm DL to combine sets of nightly images, a process that takes the median value of corresponding pixels in each image set and converts those median values into a combined image. While this process effectively removes noise from sets of images and creates clearer distinctions between stars and the background, our asteroid was too dim and fast-moving to appear in combined images. Our solution was to analyze each image individually which made our asteroid marginally easier to identify amidst the noise in our images.
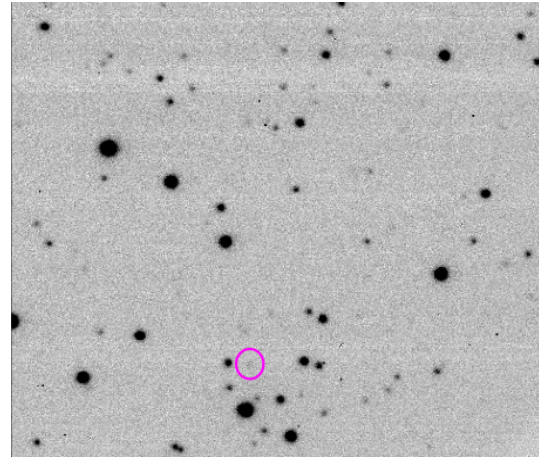
Figure 1: Sample Image Identifying 2017 BM31

2.2   Orbit Determination

Our image analyses in MaxIm DL yielded right ascension and declination data, giving us the position of the asteroid. We then employed the Gauss method of orbit determination to solve for the orbit of our asteroid. This method takes the values of right ascension and declination at three discrete times and uses those to find the equatorial position of the asteroid relative to the Sun and its velocity relative to the Sun at the middle observation.

First, the orbit of the asteroid must obey the geometric laws of the fundamental vector triangle between the Earth, Sun, and asteroid (Faison, "Making an Ephemeris"), depicted in Figure 2:
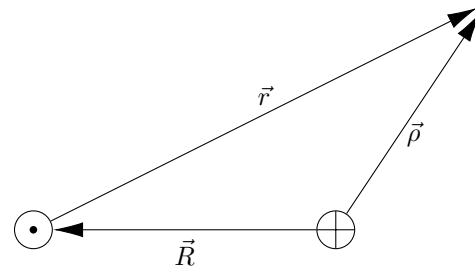
Figure 2: Fundamental Vector Triangle

The three vectors depicted in the triangle represent $\vec{R}$, the vector pointing from Earth to the Sun; $\vec{r}$, the vector from the Sun to the asteroid; and $\vec{\rho}$, the topocentric vector pointing from the observation site on the surface of the Earth to the asteroid. Due to the geometry of this configuration, we knew that the orbit of the asteroid would always behave according to the equation:

$$\vec{r} = \rho\hat{\rho} - \vec{R} \qquad (1)$$

To solve for $\vec{r}$, we needed values for all the other variables in this equation. We found $\hat{\rho}$ by:

$$\hat{\rho}_i = \langle \cos\alpha_i \cos\delta_i, \sin\alpha_i \cos\delta_i, \sin\delta_i \rangle \quad (2)$$

Meanwhile, $\vec{R}$ was obtained for each observation from the JPL DE405 Ephemeris Generator through a Python package, EphemPy (Version 1.3; Buvel 2009). Along with these geometric relationships, our method of Gauss used the generalized equation of motion for a body in an elliptical orbit around another body:

$$\ddot{\vec{r}} = \frac{-\mu\vec{r}}{r^3} \quad (3)$$

in which the terms are acceleration of the orbiting body relative to the center body in AU/modified day squared, mass of the body being orbited in solar masses, and distance between the two objects in AU. When used in conjunction with a Taylor expansion (Faison, "Numerical Integration"), the equation of motion gave us a position of the asteroid at any given time in terms of its position and velocity at the middle observation according to the f and g series:

$$f = 1 - \frac{\tau^2}{2r_2{}^3}$$
$$g = \tau - \frac{\tau^3}{6r_2{}^3} \quad (4)$$
$$r(\tau) = f\vec{r_2} + g\dot{\vec{r_2}}$$

Given these equations and unknowns, we had to input a reasonable initial guess (∼1.5 AU) for the value of r_2 in order to have all the information we needed to calculate the position vector. The method of Gauss then prescribes a specific set of vector algebra operations to perform using one's collected data that can be used to solve for the distance from the observation site on Earth to the asteroid (ρ) for each of the three observations. We then inputted into the method of Gauss as the initial guess for the distance to the asteroid at the middle observation, and then reran all the calculations until ρ_2 converged to a single value. Once we had a final calculated ρ for all three of the observations, we solved $\vec{r} = \rho\hat{\rho} - \vec{R}$ for $\vec{r}$ at all three times of observation. However, in order to be able to calculate all of the classical orbital elements, one must have both $\vec{r}$ and $\dot{\vec{r}}$, so we had to calculate the latter using Equation 5:

$$\dot{\vec{r_2}} = \frac{f_3}{g_1 f_3 - g_3 f_1}\vec{r_1} - \frac{f_1}{g_1 f_3 - g_3 f_1}\vec{r_3} \quad (5)$$

2.3   Orbit Model Optimization

To optimize our orbit model, we used our position ($\vec{r}$) and velocity ($\dot{\vec{r}}$) vectors relative to the Sun as the independent variable, and we used the goodness of fit of our model to our data as the dependent variable. To determine the goodness of fit, we used the sum of the root-mean-squares (RMS) of the residuals for right ascension and declination between our model's predictions and ran through our ephemeris generation code for RA and Dec at the same times as our recorded observations. The optimization method used was a combination of a hill-climbing/random step optimization paired with a genetic algorithm (Feddersen, "Hill Climbing"). The code makes minute and random changes to each component of $\vec{r}$ and $\dot{\vec{r}}$ and checks to see if this increases or decreases the summed RMS (whether the model got better or worse). It then returns to the previous values of $\vec{r}$ and $\dot{\vec{r}}$ if the model gets worse and taking another small random step if the fit is better. The genetic algorithm component works by generating a population of these mutated vectors and selecting the best out of those as the starting conditions on which to run the optimization code, therefore honing in on only the best fitting $\vec{r}$ and $\dot{\vec{r}}$. After running the algorithm, we saw optimistic results:
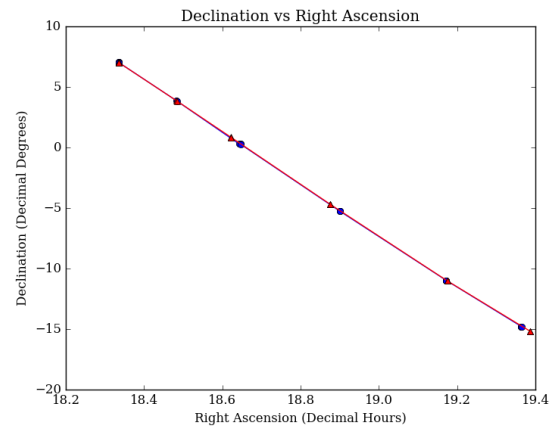
Figure 3: Optimized Orbit Model

In the figure above, the triangle plot represents our model of the asteroid's orbit and the circle plot is our recorded observations of the asteroid. Looking at the tightness of fit, it is evident that our optimization code significantly improved our model.

2.4   Osculating Orbital Elements

After the position ($\vec{r}$) and velocity ($\dot{\vec{r}}$) vectors were determined using method of Gauss, they were then used to find the osculating orbital elements based on Kepler's laws and Newton's Conservation of Momentum.

The angular momentum (h) was calculated as the cross product between the position and the velocity vectors:

$$\vec{h} = \vec{r} \times \dot{\vec{r}} \qquad (6)$$

The eccentricity (e) was then calculated using the cross product between the velocity and angular momentum vectors, and then subtracting the unit vector of position.

$$\vec{e} = (\dot{\vec{r}} \times \vec{h}) - \hat{r} \qquad (7)$$

This yielded the vector pointing in the direction of the perihelion that had a magnitude equivalent to the eccentricity. Using the eccentricity, the perihelion ($q_{perihelion}$) and aphelion ($q_{aphelion}$) distances were calculated with:

$$q_{perihelion} = \frac{|\vec{h}|^2}{1 + |\vec{e}|}$$
$$q_{aphelion} = \frac{|\vec{h}|^2}{1 - |\vec{e}|} \qquad (8)$$

The semi-major axis (α) was found by adding the perihelion distance to the aphelion distance and dividing the sum by two:

$$\alpha = \frac{q_{peri} + q_{ap}}{2} \qquad (9)$$

The inclination (i) was calculated by taking the arccosine of the z-component of $\hat{h}$, which is the unit vector of angular momentum. By taking the z-component, the angle between h and the x-y plane can be found.

$$i = \cos^{-1}(\hat{h}_z) \qquad (10)$$

To continue, an intermediate vector $\vec{N}$ was calculated to represent the vector pointing to the ascending node of the orbit, using the cross product between the z-axis and the angular momentum vector. This means that this vector $\vec{N}$ lies both on the x-y plane as it lies orthogonal to the z-axis, as well as the orbital plane. The line represents the moment where the asteroid crosses the equatorial plane on its orbit.

$$\vec{N} = \hat{z} \times \vec{h} \qquad (11)$$

The longitude of the ascending node (Ω) was calculated as the arccosine of the dot product of the unit vector $\hat{N}$ and the x-axis, which gives the angle between them. If the z-component of the angular momentum was negative, this angle was subtracted from 360° because the orbit proceeds in the opposite direction. The argument of perihelion (ω) was calculated as the arccosine of the dot product of the unit vector $\hat{N}$ and the $\hat{e}$:

$$\Omega = \cos^{-1}(\hat{N} \cdot \hat{z})$$
$$\omega = \cos^{-1}(\hat{N} \cdot \hat{e}) \qquad (12)$$

2.5   Uncertainty

The uncertainty for the osculating orbital elements takes into account the possible error caused by the telescope, which is approximately the same as the resolution of the telescope. The minimum angular separation visible under the 16-inch telescope is calculated as follows:

$$\theta = 1.220 \frac{\lambda}{d} \qquad (13)$$

where θ is the angular separation, λ is the wavelength of light being observed, and d is the diameter of the telescope. To approximate θ, we used a wavelength of 500nm to represent the visible filter, and a diameter of 0.4m for the telescope. Then, θ is 0.0087°. $\theta/15$ gives the uncertainty in hours of right ascension, and θ can be used as it is for the declination. Thus, we have calculated uncertainties by taking only one significant figure, represented here as δ_{RA} and δ_{Dec}:

$$\delta_{RA} = 0.0006$$
$$\delta_{Dec} = 0.009$$

There are four possible combinations of extreme uncertainties, $RA \pm \delta_{RA}$ and $Dec \pm \delta_{Dec}$. Using the method of Gauss, we calculated the position and velocity of the asteroid on JD 2457950.252. The orbital elements were calculated for that set of position and velocity vectors. Then, we calculated the orbital elements using all four possible combinations and subtracted the original orbital elements from those of JD 2457950.252. This gives the uncertainty in orbital elements that propagates from the uncertainty from the telescope. However, the combination of $RA - \delta_{RA}$ and $Dec - \delta_{Dec}$ resulted in a hyperbolic orbit, so it was not included in the calculation of the uncertainty of the orbital elements.

Another possible uncertainty is represented by the RMS of the residuals between our model data and our observations, and it arises from an imperfect orbit determination algorithm. The possible

uncertainty caused by an imperfect orbit determination method has not been included in the calculation of the uncertainty for the orbital elements. It is very difficult to use analytic methods to calculate the uncertainty that propagates through the method of Gauss. Therefore, the best way to determine uncertainty is to use the most extreme possible values of RA and declination to numerically find the uncertainty of orbital elements.

The RMS is useful, however, in finding the error for the RA and declination. The error bars on the RA and declination graphed over time were calculated using the RMS. We calculated the extreme RMS values using the four combinations of $RA \pm \delta_{RA}$ and $Dec \pm \delta_{Dec}$. Then, we took the average of the extreme RMS values for RA and declination as the errors for the RA and declination respectively. The error values represent the amount that the RA and declination predicted by our orbit model could be inaccurate, taking into account both the instrumental errors with the telescope as well as the imperfect orbit model. The averaged RMS values are as follows (taking only 1 significant figure):

$$RMS_{RA} = 0.02$$
$$RMS_{Dec} = 0.5$$

2.6   Long-Term Integration

The long-term trajectory of the asteroid was determined by inputting the position of velocity of the asteroid on JD 2457950.252 into the RE-BOUND Python integrator, a code developed by Rein and Liu (2012). This integrator includes the effects of Jupiter's and Earth's gravity and takes into account conservation of energy, making it a much more accurate and precise integrator than our own code which only utilized a simple fourth order Runge-Kutta integration method. We integrated forward by 10,000 years to find the minimum distance between the asteroid and the earth in the near future, and our time step was set to 0.01 modified days.

3   Results

3.1   Data From Observations

On our nights of observation, we were able to locate 2017 BM31 and find its right ascension and declination through solve-fielding. Our data is provided below:

JD	RA	Dec
2457948.8586	18h 20m 5.92s	7° 1' 41.26"
2457950.2523	18h 28m 59.84s	3° 51' 21.08"
2457951.6361	18h 38m 47.62s	0° 16' 26.73"
2457954.6210	18h 54m 1s	-5° 15' 33"
2457954.6280	18h 54m 3s	-5° 16' 16"
2457959.1115	19h 10m 20.99s	-10° 59' 3.08"
2457963.0665	19h 21m 50.99s	-14° 59' 3.08"
2457966.7766	19h 29m 44.61s	-17° 9' 33.25"

Table 1: RA & Dec from Observations

This table only displays observations that are separated by at least 10 minutes apart. The data were also collected from a variety of different telescopes (Row #1 - California; #2, 7 - Australia; #3, 4, 5, 6 - LFOP; and #8 - SMARTS).

3.2   Orbit Determination

The osculating orbital elements of 2017 BM31 were calculated from observations from 14 July to 21 July. Using the position and velocity vectors from the method of Gauss implementation, the following orbital elements were calculated:

h	1.06±0.01
e	0.15±0.02
q	0.986AU±0.002
a	1.16AU±1.03
i	21.6° ± 0.3
Ω	5.8119° ± 1.0
ω	228.4° ± 1.5

Table 2: Orbital Elements

where the position and velocity vectors were generated as:

$$\vec{r} = 0.405\hat{x} - 0.897\hat{y} - 0.370\hat{z}$$
$$\dot{\vec{r}} = 0.979\hat{x} + 0.274\hat{y} + 0.069\hat{z} \tag{14}$$

According to the REBOUND integrator, in the next 1,000 years, the asteroid arrives within 0.0136AU on JD 2768694.30804. In the next 10,000 years, the minimum distance between the asteroid and the Earth would be 0.0008AU in 3722 AD.
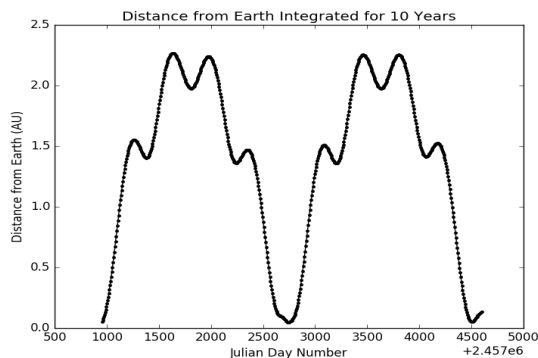
Figure 4: REBOUND Integration for 10 Years

The following figure displays the RA and declination calculated by our model for every Julian date where we made an observation. The error bars represent the possible range of the actual RA and declination values for that night.
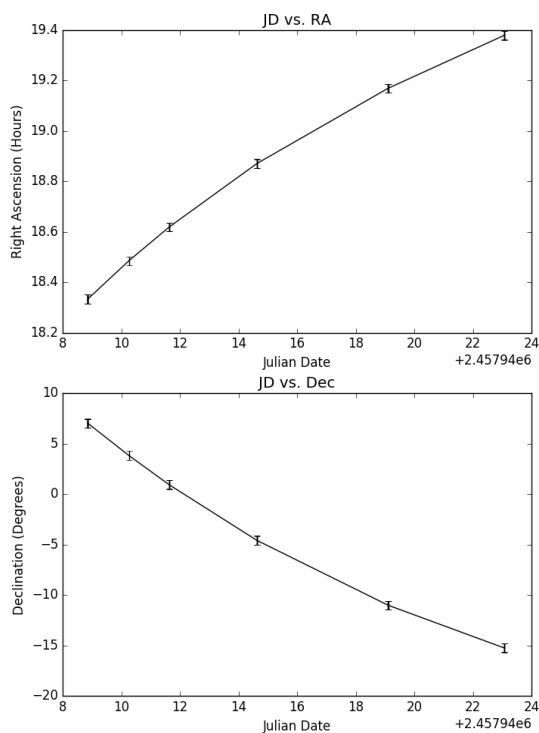
Figure 5: Modeled RA and Declination

3.3 Photometry

Collecting photometry data from 2017 BM31 was a daunting task given its low brightness, and it became more difficult as time went on since the asteroid gradually became dimmer. Because of this

and its high velocity, most images from our telescopes failed to display proper Gaussian distributions of light intensity when analyzed with MaxIm DL's photometry tool.

In an effort to find the asteroid's absolute magnitude, we analyzed one of our clearer images. Using a reference star, we calibrated the image and found the apparent magnitude:

JD	Magnitude	Phase Angle
2457950.25176	17.38	32.61°

Table 3: Magnitude & Phase Angle

Note: the phase angle was calculated through the dot product between $\vec{\rho}$ and $\vec{r}$ (see Figure 2: Fundamental Vector Triangle). We then calculated the absolute magnitude with equations from Dymock 2007:

$$H(\alpha) = V - 5\log(r\Delta)$$
$$H = H(\alpha) + 2.5\log[(1-G)\varphi_1(\alpha) + G\varphi_2(\alpha)]$$
$$\varphi_i = \exp\{-A_i(\tan 0.5\alpha)^{B_i}\}$$

$$(15)$$

where V is apparent magnitude, r is the asteroid's distance from the Sun, Δ is the asteroid's distance from the Earth, $A_1 = 3.33$, $A_2 = 1.87$, $B_1 = 0.63$, $B_2 = 1.22$, $G = 0.15$, and α is the phase angle. By plugging in the values from Table 3, we discovered that our asteroid has an absolute magnitude of 22.8.

3.4 Albedo & Size

Albedo is an intrinsic property of an asteroid which determines its reflectivity, and falls within a known range of values for the two main types of asteroids (Class C and Class S). In order to determine the class of 2017 BM31, we generated a spectrum by measuring photometric data from images taken in four wavelengths between 450 and 810 nanometers. Since most of our images were inadequate for photometry, we conducted remote observations from the more sensitive 1.3m SMARTS telescope in Chile, which gave us a better light profile.

After calibrating our images from the SMARTS telescope, we constructed a plot of 2017 BM31's relative brightness in the BVRI spectrum over time:
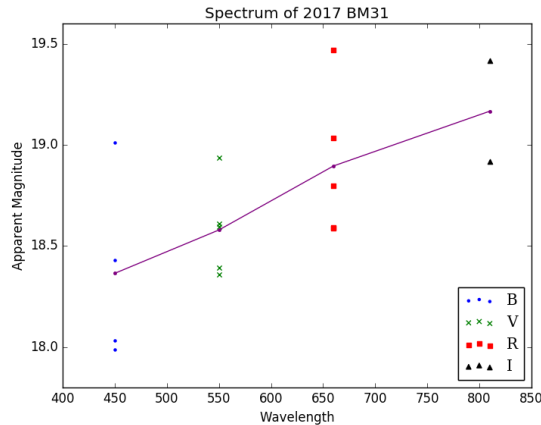
Figure 6: Spectrum of 2017 BM31

Note: SMARTS takes the pictures in multiple filter bands - B = 450nm, V = 550nm, R = 660nm, and I = 810nm.

This spectrum exhibits behavior very similar to a typical absorption spectrum for C Class carbonaceous asteroids. We then calculated the color parameter for the asteroid using those same SMARTS images and the equation:

$$a = 0.9825(v - r) + 0.3713(r - i) - 0.6204 \quad (16)$$

This yielded a value less than zero, consistent with the color parameter of C-Type asteroids. Having ascertained a range of values for the albedo of our asteroid (0.05-0.25 for a Class C), we were able to use this information to calculate an approximation of the diameter of the asteroid using the equation:

$$D = \frac{1329}{\sqrt{A}} 10^{-.2H} \quad (17)$$

where D is the diameter in kilometers, A is the albedo, and H is the absolute magnitude of the asteroid (22.8) (Faison, "Introduction to Albedo"). With our data, this equation outputs a diameter of 118 meters ± 45 meters, making 2017 BM31 a very small asteroid indeed.

3.5 Impact Assessment

In order to calculate the energy of the asteroid's impact if it were to collide with Earth, we needed to determine the two terms in the standard kinetic energy equation: mass and speed. After calculating the class and approximate diameter of the asteroid, we obtained the mass by assuming a spherical shape and using the average density of a Class C asteroid, 1.38 $\frac{g}{cm^3}$ (Krasinski et al. 2002). We then

used the Rebound Python package to run a long-term integration of our asteroid, determining when its closest approach to Earth occurs, as well as the velocity vectors of Earth and the asteroid at that time. By subtracting one of these two vectors from the other and taking the magnitude of the resulting vector, we obtained the speed of the asteroid relative to the Earth upon impact *if* the asteroid were to hit the earth at the time output by the Rebound integration as coinciding with the point of closest approach. Using the estimated size of our asteroid and the approximate density for its class we calculated a mass of about 3 billion kilograms and the Rebound integration gave us an impact speed of 48 $\frac{km}{sec}$. Substituting these values into the equation for kinetic energy results in a whopping 3×10^{15} kilojoules of energy, equivalent to the energy of 850 megatons of TNT (over fifteen times the destructive power of the largest nuclear bomb produced to date).

4 Discussion

We have found 2017 BM31 to be an incredibly small and dim asteroid, with a diameter around a measly 118 meters and an absolute magnitude of 22. One of the most remarkable traits of this asteroid, however, is how similar its orbit is to Earth's; 2017 BM31 has an eccentricity almost identical to that of Earth, a semimajor axis of nearly 1 AU, and an almost nonexistent inclination. While its path currently takes it well out of Earth's orbit, the threat 2017 BM31 poses to Earth in the future is not negligible. Our models have predicted that in the year 3722 it may approach as close as two lunar distances away, and its path crosses or comes very close to that of Earth with every rotation around the Sun. One might be tempted to discount the asteroid's impact in the event of a collision due to its relatively small size, but what it lacks in size it more than makes up for in speed, meaning that the energy dissipated in a collision would be enough to enact serious damage upon the planet.

Interestingly, our orbit model is very different from the model generated by JPL Horizons, which has a much greater semi-major axis and eccentricity. This discrepancy may have arisen from the fact that multiple orbits could be fitted to a set of observations, especially if the time span of the observations is relatively short. The observations we made over 3 weeks may have yielded a close approximation to the asteroid's position and velocity based on these observations. However, they may

have been trapped on a "hill of optimization" where the orbital model we calculated is relatively fit to our observations, but there is a better model that is drastically different. Using the hill-climbing optimization method, we would not be able to reach the better model from our method of Gauss optimization because moving in any direction would lead to a decrease in goodness of fit. Our method is thus confined to a local maximum and unable to reach the global one. This represents a limitation in our observations and orbit determination methods. This may account for the high RMS value of around 0.02 hours for the right ascension and 0.3° for the declination.

Additionally, the possible uncertainty caused by the centroid and astrometry algorithms were not taken into account when assessing the overall uncertainty of our orbit determination. Further improvements would involve more extensive numerical tests for the uncertainties due to centroid, astrometry, or instrumental inaccuracies. These uncertainties may factor a large role in our orbit determination, as slight changes in our calculated initial conditions could yield extremely different results.

For example, certain points of RA and declination that lie within the instrumental error range yield orbits that do not converge. Although our model fits our observations with reasonable accuracy for the duration of YSPA, more distant data points would help ensure that our orbit model is not simply one that happens to fit the data closely. Parallax observing would increase the accuracy of the initial guess for position, making it more likely to determine the true orbit. The findings presented in this paper represent a model best fit to this range of observations, and a more accurate model can only be found with more extensive observations of 2017 BM31.

5   Acknowledgments

References

[1] Buvel R. 2009. EphemPy (Version 1.3) [Computer software]. Cambridge, Massachusetts: Massachusetts Institute of Technology

[2] Dymock, R. 2007, JBAA, 117, 342D.

[3] Faison, M. D. "Introduction to Albedo and Diameter Matching." July 2017.

[4] Faison, M. D. "Making an Ephemeris (RA and Dec) from the Vector Orbital Elements." July 2017.

[5] Faison, M. D. "Numerical Integration with the f and g Series." July 2010.

[6] Feddersen, J. "Hill Climbing - You're getting warmer!" July 2017.

[7] George, D., Sharratt, G., Benson, E., et al. 2001. MaxIm DL: CCD Imaging Software (Version 3.04) [Computer software]. Ottawa, Ontario: Diffraction Limited.

[8] Joye W., Mandel E., Murray S., et al. 2015. SAOImage DS9 (Version 7.4) [Computer software]. Cambridge, Massachusetts: Smithsonian Astrophysical Observatory.

[9] Krasinsky, G. A., Pitjeva, E. V., Vasilyev, M. V., & Yagudina, E. I. 2002, , 158, 98

[10] Lang D., Hogg D. W., Mierle K., et al. 2010, AJ, 139, 1782.

[11] Popova O. P., Jenniskens P., Emel'yanenko V., et al. 2013. "Chelyabinsk Airburst, Damage Assessment, Meteorite Recovery, and Characterization." *Science*.

[12] Rein H., Liu S. 2009. REBOUND (Version 3.2.2) [Computer software]. Toronto, Canada: University of Toronto.